Available online at www.sciencedirect.com
ScienceDirect
Proceedings of the Combustion Institute 31 (2007) 2463–2471
Proceedings of the Combustion Institute
www.elsevier.com/locate/proci

Numerical simulations of flame propagation and DDT in obstructed channels filled with hydrogen–air mixture

Vadim N. Gamezo [a,*], Takanobu Ogawa [b], Elaine S. Oran [a]

[a] Laboratory for Computational Physics and Fluid Dynamics, Naval Research Laboratory, Washington, DC 20375, USA
[b] Department of Mechanical Engineering, Seikei University, 3-3-1 Kichijoji-Kitamachi, Musashino-shi, Tokyo 180-8633, Japan

Abstract

We study flame acceleration and deflagration-to-detonation transition (DDT) in channels with obstacles using 2D and 3D reactive Navier–Stokes numerical simulations. The energy release rate for the stoichiometric H_2–air mixture is modeled by a one-step Arrhenius kinetics. Computations show that at initial stages, the flame and flow acceleration is caused by thermal expansion of hot combustion products. At later stages, shock–flame interactions, Rayleigh–Taylor, Richtmyer–Meshkov, and Kelvin–Helmholtz instabilities, and flame–vortex interactions in obstacle wakes become responsible for the increase of the flame surface area, the energy-release rate, and, eventually, the shock strength. Computations performed for different channel widths d with the distance between obstacles d and the constant blockage ratio 0.5 reproduce the main regimes observed in experiments: choking flames, quasi-detonations, and detonations. For quasi-detonations, both the initial DDT and succeeding detonation reignitions occur when the Mach stem, created by the reflection of the leading shock from the bottom wall, collides with an obstacle. As the size of the system increases, the time to DDT and the distance to DDT increase linearly with d^2. We also observe an intermediate regime of fast flame propagation in which local detonations periodically appear behind the leading shock, but do not reach it.

Keywords: DDT; Hydrogen; Modeling

1. Introduction

Channels with obstacles are often used to study the flame acceleration and the deflagration-to-detonation transition (DDT) in a controlled manner [1–14]. The basic experimental setup consists of a round or rectangular tube filled with a combustible gaseous mixture and closed at one end. A number of evenly spaced obstacles inside the tube partially obstruct flow through the channel. A laminar flame, ignited near the closed end of the channel, quickly accelerates, and becomes turbulent. Analysis of experimental data shows [1,11] that the turbulent flames in channels with obstacles can accelerate to supersonic velocities, or remain subsonic and possibly quench. There are three different regimes for quasi-steady-state supersonic flame propagation [1]: choking, quasi-detonation, and detonation.

* Corresponding author. Fax: +1 202 767 6260.
E-mail address: gamezo@lcp.nrl.navy.mil (V.N. Gamezo).

1540-7489/$ - see front matter © 2006 The Combustion Institute. Published by Elsevier Inc. All rights reserved.
doi:10.1016/j.proci.2006.07.220

In the choking regime, the flame is decoupled from the leading shock and spreads through the molecular or turbulent transport and convection. The flame speed in the laboratory frame of reference is typically from 1/3 to 1/2 of the Chapman-Jouguet (CJ) detonation velocity D_{CJ} and often close to the sound speed in the combustion products.

In the quasi-detonation regime, the shock and the flame are coupled at some times and locations where the reaction is triggered directly by the shock compression. At other times and locations, the shock and the flame decouple as the detonation diffracts over the obstacles. Quasi-detonations usually propagate faster than choked flames, and they are observed when the width of unobstructed part of the channel d is larger than a few detonation cell sizes λ [3,8]. The propagation velocity increases with d/λ and reaches D_{CJ} when the detonation propagation becomes independent of diffraction effects. Transitions from the choking to the quasi-detonation regime are routinely observed [1–12], but the mechanism of this transition is not well understood.

Fundamental DDT theory [15,16] and simulations [17,18] suggest that a detonation may develop from a spontaneous reaction wave propagating through a reactivity gradient. It is unclear, however, how and where this gradient forms in channels with obstacles. One possibility is a mixing of unreacted and reacted materials in turbulent flow that extinguishes the flame and creates concentration and temperature gradients [3]. Another possibility is the shock compression of the unreacted material. Hot spots resulting from shock–shock, shock–wall, and shock–vortex interactions contain temperature gradients that produce spontaneous waves and detonations [17–20]. The shock compression scenario is favored by the results of experiments [5–7] in which transition to quasi-detonation was suppressed when shock reflections at the channel walls were damped by wire screens.

Transition to detonation was not included in numerical simulations of subsonic and choking regimes in obstructed channels [13,14]. Shock–flame interactions and DDT in channels without obstacles were successfully modeled in [17–20]. In the work presented here, we use numerical techniques [17–20] to study the flame acceleration and DDT in channels with obstacles.

2. Numerical and physical model

The numerical model is based on reactive Navier–Stokes equations coupled with the ideal-gas equation of state and a one-step Arrhenius kinetics of energy release, $\mathrm{d}Y/\mathrm{d}t = -A\rho Y \exp(-E_a/RT)$, where Y is the unburned mass fraction, A is the pre-exponential factor, and E_a is the activation energy. The equations are solved using an explicit, second-order, Godunov-type numerical scheme, and an adaptive mesh [21]. This model has been extensively tested and used to solve combustion and detonation problems including shock–flame interactions and DDT [17–20], propagation of laminar flames [22], and cellular detonations [23–25].

System parameters summarized in Table 1 approximately correspond to the stoichiometric H_2–air mixture at 1 atm and 293 K. The table also shows computed properties of ideal one-dimensional (1D) steady-state flames and detonations for this system. The laminar flame thickness x_l and flame speed S_l were computed from the numerical model described above, where x_l was defined as the distance between $Y = 0.1$ and $Y = 0.9$ planes. We used the steady-state Zeldovich-von Neumann-Doering (ZND) solution to compute the half-reaction thickness of the 1D detonation wave x_d, defined as the distance between the shock and the $Y = 0.5$ plane.

The detonation cell size λ is often measured in experiments, correlates with the theoretical parameter x_d [26], and used in empirical correlations related to the detonation initiation and DDT [1–14]. To estimate λ for our system, we computed detonation propagation in 2D channels without obstacles. These computations used an adaptive mesh with the minimum computational cell size $\mathrm{d}x_{\min} = 1/2048$ cm, corresponding to 39 computational cells per half-reaction thickness. The resulting cellular patterns are very irregular and contain two levels of detonation cells, as expected for the high activation energy $E_a/RT_{ZND} = 13.4$ [23–25,27]. Large cells are 1–2 cm wide, which corresponds to 50–100 x_d, and is close to experimental values of $\lambda = 1.1-2.1$ cm [26].

The one-step Arrhenius kinetics used in this model cannot reproduce all properties of H_2–air mixture for different combustion regimes, including laminar flames, detonations, and DDT. The model does, however, provide approximately correct length and time scales for the problem considered. This allows us to use this model for a qualitative analysis of the behavior of H_2–air mixture.

3. Two-dimensional simulations

The setup for 2D simulations is schematically shown in Fig. 1. The channel closed at the left end, open at the right end, and partially obstructed by rectangular obstacles $O_1, O_2, \ldots, O_n$ evenly spaced along the whole channel length L. The obstacle height $d/4$ corresponds to the blockage ratio 0.5, which is kept constant as we vary the width of the computational domain $d/2$ from 1 to 8 cm. The channel is filled with the stoichiometric H_2–air mixture described above. We ignited a flame by placing a circular region of hot burned

Table 1
Input model parameters and computed properties of reaction waves for stoichiometric hydrogen–air mixture

P_0	1 atm	Initial pressure
T_0	293 K	Initial temperature
ρ_0	8.7345×10^{-4} g/cm^3	Initial density
γ	1.17	Adiabatic index
M	21 g/mol	Molecular weight
A	6.85×10^{12} cm^3/g-s	Pre-exponential factor
E_a	$46.37RT_0$	Activation energy
q	$43.28RT_0/M$	Chemical energy release
$\nu_0 = \mu_0 = D_0$	2.9×10^{-5} g/s-cm-K$^{0.7}$	Transport constants
S_l	298 cm/s	Laminar flame speed
T_b	7.289 T_0	Post-flame temperature
ρ_b	0.1372 ρ_0	Post-flame density
x_l	0.035 cm	Laminar flame thickness
D_{CJ}	1.993×10^5 cm/s	CJ detonation velocity
P_{ZND}	31.47 P_0	Post-shock pressure
P_{CJ}	16.24 P_0	Pressure at CJ point
T_{ZND}	3.457 T_0	Post-shock temperature
T_{CJ}	9.010 T_0	Temperature at CJ point
ρ_{ZND}	9.104 ρ_0	Post-shock density
ρ_{CJ}	1.802 ρ_0	Density at CJ point
x_d	0.01927 cm	Half-reaction thickness
λ	1–2 cm	Detonation cell size

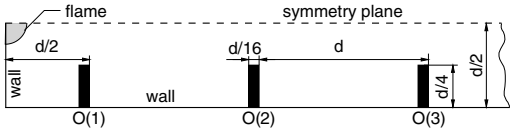

Fig. 1. Computational setup. Obstacles $O_1, O_2, \ldots, O_n$ are evenly spaced along the whole channel length L. Walls and obstacle surfaces are no-slip reflecting boundaries. Initial flame radius is 0.5 cm.

material near the closed end of the channel at $t = 0$. Now we describe in detail the case for $d/2 = 2$ cm computed with a high numerical resolution, and then discuss resolution tests, the effect of ignition mode, and the effect of channel width.

3.1. Flame evolution for d/2 = 2 cm

Simulations for $d/2 = 2$ cm and $L = 64$ cm were performed with the minimum computational cell size $dx_{min} = 1/512$ cm. The resulting flame and the flow development is shown in Fig. 2 by a time sequence of temperature fields. Each frame shows only a 10.7 or 5.3 cm section of the computational domain adjacent to the leading reaction front.

The laminar flame, ignited at the left top corner of the computational domain, propagates with the velocity close to $S_l = 298$ cm/s relative to unburned material. Hot reaction products expand and push unreacted material towards the open end of the channel. The flame front propagates with the moving flow and quickly becomes very convoluted as the flow interacts with obstacles. The increasing flame surface area results in faster energy release, thus accelerating the flow and increasing the flame speed in the laboratory frame of reference. This basic mechanism of flame acceleration does not require turbulence [11] and is similar to the mechanism of laminar flame acceleration in narrow channels without obstacles [22,28].

As the flame passes obstacles, it wrinkles due to the Rayleigh–Taylor (RT) instability caused by the flow acceleration. The unreacted flow ahead of the flame becomes sonic by 1.4 ms, just past O_5. Noticeable shocks begin to form ahead of the flame past O_7 at 1.85 ms. They reflect from obstacles and side walls, and interact with the flame triggering Richtmyer–Meshkov (RM) instabilities. Kelvin–Helmholtz (KH) instabilities develop at the flame surface when a jet of hot burned material passes through a narrow part of the channel and a shear layer forms downstream of the obstacle. RT, RM, and KH instabilities, and flame–vortex interactions in obstacle wakes are the mechanisms responsible for increases in flame surface area, energy-release rate, and, eventually, shock strength. The elevated temperature behind shocks also contributes to the increased energy-release rate because S_l increases and shocks passing through the reaction zone release additional energy.

The average flame velocity gradually increases and reaches 800 m/s by 2.1 ms. This velocity

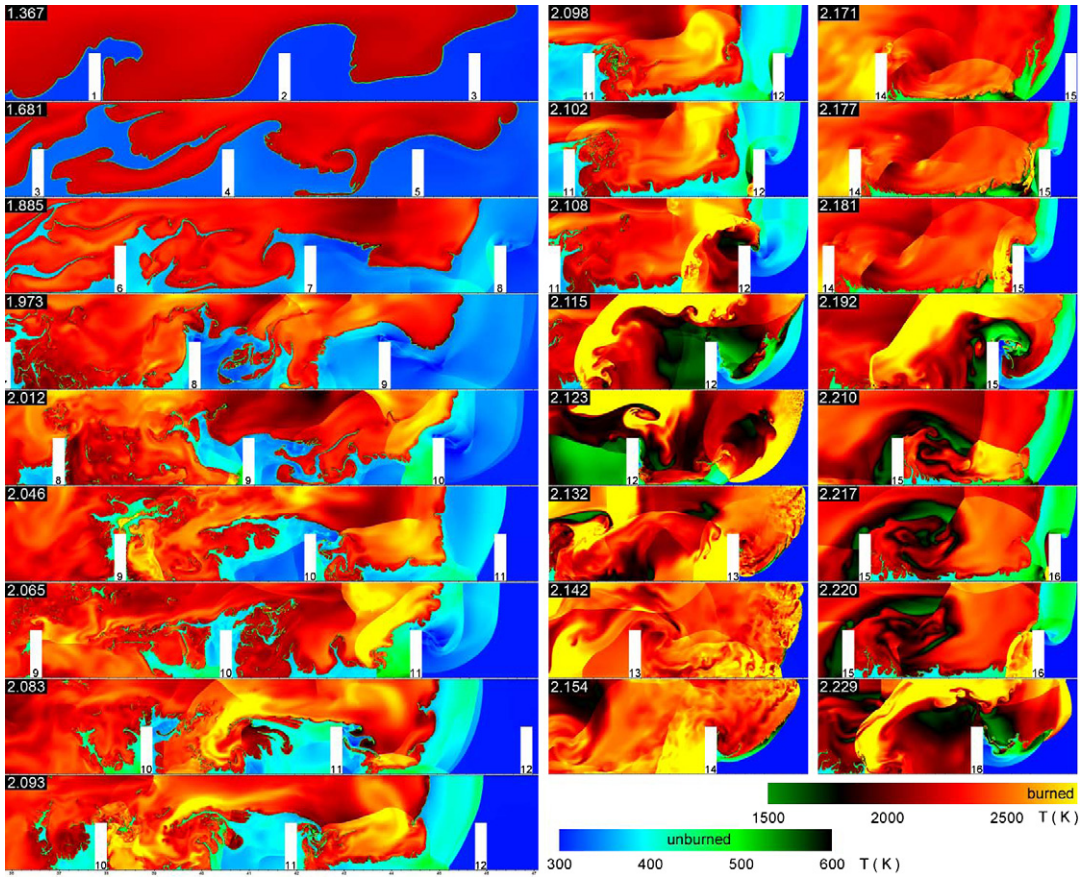

Fig. 2. Accelerating flame (left column), DDT, and quasi-detonation (two right columns) in 2D half-channel with obstacles computed for $d/2 = 2$ cm, $L = 64$ cm, $\mathrm{d}x_{\min} = 1/512$ cm. Times in milliseconds are shown in frame corners.

equals about 0.8 of sound speed in the burned material, or 0.4 D_{CJ}, and is typical of what has been called the choking regime of flame propagation [1] observed in experiments with obstructed channels. The term "choking regime" introduced in [1] suggests that the flame speed is controlled by the gasdynamic choking of the flow. Even though this suggestion provides a plausible explanation for observed flame speeds that are close to the sound speed in the burned material, there is no direct experimental evidence of choking flow conditions occurring behind fast flames in channels with obstacles [7]. To investigate this issue, we computed local Mach numbers in the laboratory frame of reference for different times. A typical flow field, such as shown in Fig. 3, contains one or several large supersonic regions in the burned material at some distance behind the leading edge of the flame. The supersonic flow regions do not correlate with obstacle locations, and extend to the left roughly as far as the major energy-release zone. The flow speed in these regions can exceed Mach 2, but this flow does not interact directly

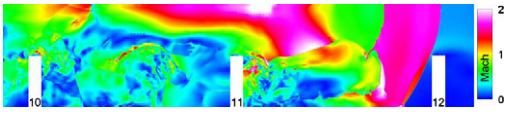

Fig. 3. Mach number of the reactive flow in channel with obstacles at 2.093 ms. Temperature for the same flow field is shown in Fig. 2. Mach number is computed in the laboratory frame of reference using the local sound speed, which is ~370 m/s for cold material, 420–470 m/s for unreacted shock-compressed material, and 980–1180 m/s for burned gas. Velocity of the leading edge of the flame ~800 m/s. $d/2 = 2$ cm.

with the leading edge of the flame that propagates with a slower flow at ~800 m/s. Thus, our results show no evidence of any choking conditions.

As the shock and the flame accelerate, the leading edge of the flame remains about 1 cm behind the leading shock, which diffracts at every obstacle and reflects from the bottom wall after each diffraction. The reflection type changes from regular to strong as the reflection point approaches the

next obstacle. The resulting Mach stem becomes stronger after each diffraction, and the temperature of the hot region that forms when the Mach stem collides with an obstacle increases. At 2.100 ms, the reflection of the Mach stem from O_{12} creates a region with temperatures above 830 K. Two hot spots in this region ignite producing two small flame kernels. Then a detonation appears near one of the kernels and propagates through the unreacted material.

Detailed numerical studies of detonation initiation in hot spots [17,18] showed that spontaneous reaction waves propagating through temperature gradients create both new flames and detonations. A detonation appears when the gradient profile allows the source of chemical energy to travel for some time with the same speed as the shock wave generated by the energy release, so the shock can be amplified to a detonation strength [15,16]. If this does not happen, the hot-spot explosion produces a flame. The shock wave propagating into surrounding hot material can trigger additional hot-spot explosions that can eventually initiate a detonation, as we observe here.

The newly formed detonation propagates through the gap between the flame and the obstacle into the shock-compressed material ahead of the flame. As the detonation passes around the obstacle, the lower part of the front decouples into a separated shock and a flame. The upper part of the front remains essentially undisturbed and develops detonation cells before it collides with the upper boundary. The collision creates a strong reflected shock that triggers a detonation in both the shock-compressed layer between the leading shock and the decoupled flame, and the uncompressed material. The strong detonation wave in the uncompressed material quickly develops detonation cells, collides with O_{13} at 2.125 ms, and diffracts. As the diffraction weakens the detonation wave, detonation cells grow and form an irregular two-level structure. The diffraction on O_{14} completely decouples the shock and flame by 2.164 ms, and effectively kills the detonation. A new detonation is ignited in the shock-compressed material by the collision of the Mach stem with O_{15} at 2.179 ms, but this detonation is unable to propagate through the very narrow gap between the obstacle and the flame. The leading shock and the flame remain decoupled until the Mach stem hits O_{16} and triggers a new detonation at 2.217 ms that spreads past the obstacle. Detonation reignition by the collision of a Mach stem with an obstacle is one of reignition mechanisms observed in experiments [7].

Experimental diagnostics for experiments analogous to those modeled here usually involve measurements of flame and shock positions as functions of time. Figure 4 shows these and global energy release data from our simulations. The flame

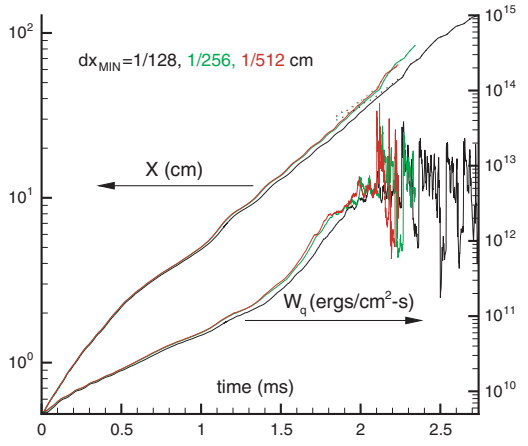

Fig. 4. Positions of flame (solid lines) and shock (dots), and global energy release rate W_q as functions of time computed for $d/2 = 2$ cm for three different numerical resolutions. W_q is scaled by $d/2$. Soft ignition mode.

position is defined as the maximum x, where the unburned mass fraction drops below 0.5. The shock position is defined as the maximum x where the pressure increases above 1.5 P_0. These positions are computed at every timestep with the uncertainty of dx_{min}. The flame acceleration, shock formation, transition to quasi-detonation, flame decoupling, and detonation reignition can be identified from these data. The global energy release peaks when the detonation appears in the system, and shock and flame positions merge when the detonation reaches the leading shock.

Similar quasi-detonation regimes that involve the detonation diffraction, failure, and reignition are often observed in experiments when the width of the narrow part of the channel d_O is larger than a few λ [3,8]. In our simulations, $d_O = 2$ cm is comparable to $\lambda = 1-2$ cm.

3.2. Effect of numerical resolution

We computed the same flame-propagation problem for $d/2 = 2$ cm using three different numerical resolutions with $dx_{min} = 1/128$, 1/256, and 1/512 cm. These resolutions correspond to 4.5, 9, and 18 computational cells per $x_l = 0.035$ cm at 1 atm, or 2.5, 5, and 10 cells per $x_d = 0.01927$ cm. For the low- and medium-resolution cases, the channel was 128 cm long, twice the length of the high-resolution case described above.

Figure 4 shows that there are only minor effects of numerical resolution on the flame acceleration and the energy-release rate. The initial flame development is actually very similar for all cases. There is a slight difference in the flame behavior in high-vorticity areas, such as obstacle wakes. The higher the numerical resolution, the more

often we see small pieces of flames separated from the bulk of burned material as a result of flame-vortex interactions. These flamelets grow and coalesce with the main flame, except in the highest-resolution case where some are extinguished. These phenomena occur only occasionally and do not produce distributed flame structures. Isolated extinguished flames mix burned and unburned materials on small scales, but we do not observe any ignition phenomena related to this mixing. This result may change if computations are performed with the significantly higher numerical resolution needed to capture details of turbulent burning in distributed regime. Therefore, our results do not exclude the mixing as a possible mechanism for DDT in channels with obstacles discussed in [3].

Even though we do not resolve the distributed turbulent burning that may occur in wakes of obstacles, we observe a very convoluted flame surface in these regions. There are many funnels and pockets of unburned material surrounded by hot burning products. These pockets and funnels burn quickly because of multiple shock reflections and shock–flame interactions. Shocks propagating through this turbulent flame brush strengthen and eventually contribute to the flow acceleration. These phenomena are observed for all numerical resolutions and may account for "the autoignition in large recirculating eddies in the wake of obstacles" reported in experiments [7].

For all numerical resolutions, DDT occurs only near left bottom corner of obstacles in hot spots generated by shock reflections. For $\mathrm{d}x_{\min} = 1/512$ and $1/256$ cm, the detonation appears at 2.10 and 2.12 ms, respectively, at the same location near the corner of O_{12}, and spreads past the obstacle. For $\mathrm{d}x_{\min} = 1/128$ cm, the first DDT event occurs at 2.22 ms in the corner of O_{13}, but it is unsuccessful and produces only a flame kernel. The detonation appears only when the shock collides with the corner of O_{14} obstacle at 2.26 ms.

The quasi-detonation regime is qualitatively the same for all resolutions, even though there are slight differences in detonation diffraction phenomena. In particular, the two-level detonation cellular structure is less pronounced for the medium-resolution case, and only one level of detonation cells is observed for the low-resolution case. Whereas the lowest resolution is insufficient to model detonation structures accurately, it is adequate for studying flame acceleration that creates conditions for the onset of detonation.

The actual formation of the detonation wave through the gradient mechanism is affected by the numerical resolution in the sense that the fine structure of hot spots changes with resolution. For example, higher-resolution computations may reveal several small ignition spots instead of one observed in lower-resolution computations. This has a minor effect, however, on the ability of the detonation to appear at this particular location because hot spots in our computations are produced by reflections of strong shocks at obstacles. Thus the obstacles set the locations where a detonation can appear. Whether the detonation will appear at a particular obstacle is mostly determined by the strength of the leading shock that develops during the flame acceleration stage. The details of detonation development from a hot spot can affect the time and location for detonation initiation only if the strength of a shock colliding with an obstacle happens to be marginal.

3.3. Effect of ignition mode

We change the ignition mode by adding energy into the initial burned region at $t = 0$. Here, the energy added per unit mass was 25 times larger than the chemical energy release q, corresponding to spark ignition powerful enough to create a strong shock, but not to ignite a detonation. Computations performed for $d/2 = 2$ cm and $\mathrm{d}x_{\min} = 1/128$ cm show the same processes of flame acceleration and transition to quasi-detonation as observed for the "soft" ignition without the additional energy. As before, the transition to the quasi-detonation regime occurs near the corner of O_{14}, but the time to DDT is reduced to 0.84 ms from 2.26 ms for the soft ignition.

The main difference between the soft and spark ignitions is that the extra energy causes more initial expansion, thus increasing the initial flow acceleration. A strong shock created at the beginning of this expansion reflects from obstacles and channel walls and perturbs the flame, thus increasing the flame surface area and the energy-release rate. As a result, the DDT occurs sooner. Flame and shock positions, and the global energy-release rate for the spark ignition case are shown Fig. 5.

We observe two DDT events preceding the transition to the quasi-detonation. They occur at 0.61 and 0.76 ms at the left side of O_8 and O_{11}, about 4.5 cm behind the leading edge of the flame. These detonations do not spread past the obstacles where they originate, and have a little effect on the propagation of the leading edge of the flame.

3.4. Effect of channel width

We computed the spark-ignited flame propagation for $d/2 = 1$, 2, 4, and 8 cm. Obstacle sizes and spacing were changed in proportion to d. Flame and shock positions, and the global energy-release rate are shown as functions of time in Fig. 5.

For $d/2 = 1$ cm, we observed 14 DDT events triggered by shock reflections in corners. The first one, at O_{22}, 0.559 ms, and the last one, at O_{55}, 1.245 ms, were unsuccessful and produced flames. Others produced detonations, but only in three

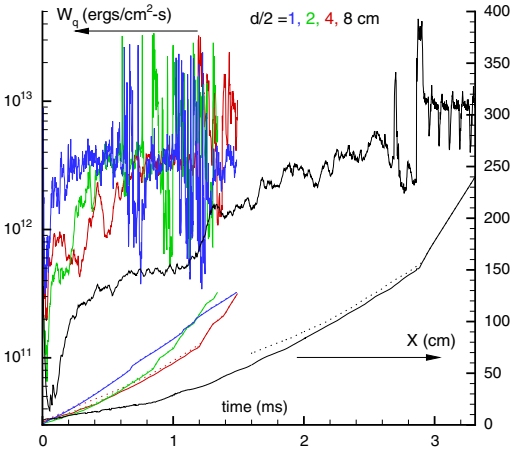

Fig. 5. Positions of flame (solid lines) and shock (dots), and global energy release rate W_q as functions of time computed for four different channel widths. W_q is scaled by $d/2$. $\mathrm{d}x_{\min} = 1/128$ cm. Spark ignition mode.

cases (at 0.665, 1.062, and 1.154 ms) were detonations able to reach and overcome the leading shock. In all three cases, the detonation wave survived only one diffraction on the next obstacle before it decoupled into a shock and a flame. For most of the time, the flame propagated in the choking regime, staying about 0.5 cm behind the leading shock.

For $d/2 = 4$ cm, the detonation appears at 1.190 ms at the corner of O_{10} and spreads past the obstacle into unburned material ahead of the flame. The detonation survives the diffraction on O_{11}, but the flame decouples from the shock by 1.323 ms, when the shock reaches O_{13}. Shock reflection at the bottom wall between O_{13} and O_{14} at 1.377 ms reignites the detonation which propagates past O_{15} and O_{16} to the end of the channel. This quasi-detonation regime is similar to that observed for $d/2 = 2$ cm.

For $d/2 = 8$ cm, a detonation first appears at 2.690 ms at the corner of O_8, 16 cm behind the leading edge of the flame. This detonation does not spread past the obstacle. Then two DDT events occur at O_9 and O_{10} at 2.870 and 2.860 ms, respectively. The detonation originating from O_{10} overtakes the leading shock and propagates to the end of the channel with an average velocity close to D_{CJ}. Detonation diffraction phenomena that occur beyond O_{10} have a little effect on the propagation of the central part of the detonation front. Only a limited local flame decoupling is observed at the bottom part of the diffracting front.

Changing $d/2$ from 1 to 8 cm thus produces all of the main regimes of fast flame propagation in channels with obstacles observed in experiments: choking flames, quasi-detonations, and detonations. In all cases, the DDT is triggered by shock

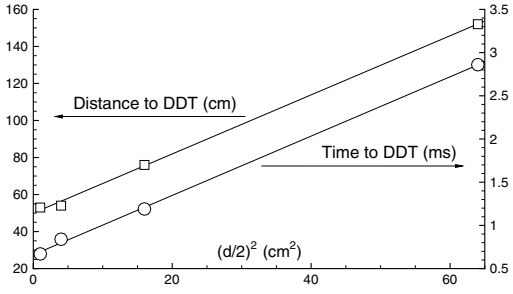

Fig. 6. Time and distance to DDT as functions of channel width from 2D results shown in Fig. 5. Points correspond to first DDT events that lead to the coupling between the leading shock and the flame.

reflections at corners between obstacles and the bottom wall when the leading shock becomes strong enough. As the size of the system increases, the time to DDT and the distance to DDT increase linearly with d^2 (Fig. 6).

4. Three-dimensional simulations

We computed one 3D case using a rectangular computational domain $64 \times 1 \times 1$ cm and $\mathrm{d}x_{\min} = 1/128$ cm to study the effect of dimensionality on simulation results. The computational setup for 3D simulations is similar to the 2D setup shown in Fig. 1. Boundary conditions at $z = 0$ and $z = 1$ cm are free-slip reflecting walls. Rectangular obstacles that touch these walls do not introduce any additional perturbations compared to the 2D setup. A cylindrical flame centered at $x = 0$, $y = 1$ cm was initialized using the spark ignition mode with an additional energy deposited into burned material at $t = 0$. Small sinusoidal perturbations were imposed on the flame surface in the third dimension.

Computational results show a very similar flame development for 2D and 3D cases. Even though the 3D flame becomes very convoluted in the third dimension, the overall flame development is dominated by shock reflections on flat obstacles and the KH instability of flat shear layers in obstacle wakes. As a result, the time evolution of global energy-release rates and positions of the flame and the shock are very similar for 2D and 3D cases as shown in Fig. 7.

The difference is that the leading shock in 3D case always remains decoupled from the flame because DDT events occur at ~2 cm behind the leading edge of the flame. This difference may be related to the fact that the leading shock colliding with flat obstacles in 3D simulations is slightly non-planar, but it may also be related to a stochastic nature of turbulent flame propagation and DDT. A limited amount of data presented here does not allow us to determine if slight differ-

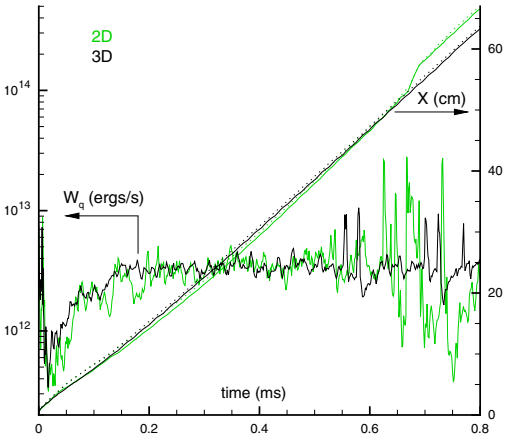

Fig. 7. Positions of flame (solid lines) and shock (dashed lines), and global energy release rate W_q as functions of time computed for 2D and 3D cases. $d/2 = 1$ cm, $dx_{min} = 1/128$ cm. Spark ignition mode.

ences between 2D and 3D results are statistically significant.

5. Conclusions

Numerical simulations described here show details of flame acceleration, detonation initiation, and propagation of turbulent flames and detonations in channels with obstacles. At initial stages, the flame and flow acceleration is caused by thermal expansion of hot combustion products. At later stages, shock–flame interactions, RT, RM, and KH instabilities, and flame-vortex interactions in obstacle wakes become responsible for the increase of the flame surface area, the energy-release rate, and, eventually, the shock strength.

When the leading shock becomes strong enough, detonations appear from hot spots created by shock reflections at corners between obstacles and the wall. As the size of the system increases, the time to DDT and the distance to DDT increase linearly with d^2. Both the initial DDT starting the quasi-detonation regime, and succeeding detonation reignitions occur when the Mach stem, created by the reflection of the leading shock from the bottom wall, collides with an obstacle. The same reignition mechanism was observed in experiments [7].

Simulations reproduce the main regimes observed in experiments: choking flames, quasi-detonations, and detonations. For the choking regime, we observe substantially supersonic (~2 km/s) flows of burned material behind the leading edge of the flame that propagates at ~800 m/s, and find no evidence of actual gasdynamic choking. We also observe an intermediate regime of fast flame propagation in which local detonations periodically appear behind the leading shock, but do not reach it. The small difference between 2D and 3D results indicates that key physical phenomena responsible for the flame acceleration and propagation in choking regime may be essentially the same in two and three dimensions.

Acknowledgments

This work was supported in part by Japan's New Energy and Industrial Technology Development Organization (NEDO) in cooperation with Shumizu Corporation, the NASA ATP program (NRA-02-OSS-01-ATP), and by the Naval Research Laboratory (NRL) through the Office of Naval Research. Computing facilities were provided by the DOD HPCMP program.

References

[1] J.H. Lee, R. Knystautas, C.K. Chan, *Proc. Combust. Inst.* 20 (1985) 1663–1672.
[2] Y.K. Liu, J.H. Lee, R. Knystautas, *Combust. Flame* 56 (1984) 215–225.
[3] O. Peraldi, R. Knystautas, J.H. Lee, *Proc. Combust. Inst.* 22 (1988) 1629–1637.
[4] R. Knystautas, J.H.S. Lee, J.E. Shepherd, A. Teodorczyk, *Combust. Flame* 115 (1988) 424–436.
[5] A. Teodorczyk, J.H. Lee, R. Knystautas, *Proc. Combust. Inst.* 22 (1988) 1723–1731.
[6] A. Teodorczyk, J.H.S. Lee, R. Knystautas, *AIAA Prog. Astronaut. Aeronaut.* 133 (1990) 233–240.
[7] A. Teodorczyk, *Biuletyn Instytutu Techniki Cieplnej Politechniki Warszawskiej* 79 (1995) 145–178.
[8] M.S. Kuznetsov, V.I. Alekseev, S.B. Dorofeev, *Shock Waves* 10 (2000) 217–223.
[9] S.B. Dorofeev, M.S. Kuznetsov, V.I. Alekseev, et al., *J. Loss Prevent. Proc. Indust.* 14 (2001) 583–589.
[10] V.I. Alekseev, M.S. Kuznetsov, Y.G. Yankin, et al., *J. Loss Prevent. Proc. Indust.* 14 (2001) 591–596.
[11] S.B. Dorofeev, *Journal de Physique IV* 12 (2002) 3–10.
[12] M.S. Kuznetsov, V.I. Alekseev, Y.G. Yankin, S.B. Dorofeev, *Combust. Sci. Technol.* 174 (2002) 157–172.
[13] A. Veser, W. Breitung, S.B. Dorofeev, *Journal de Physique IV* 12 (2002) 333–340.
[14] W. Breitung, S. Dorofeev, A. Kotchourko, et al., *Nucl. Eng. Des.* 235 (2005) 253–270.
[15] Ya.B. Zeldovich, V.B. Librovich, G.M. Makhviladze, G.I. Sivashinsky, *Astronaut. Acta* 15 (1970) 313–321.
[16] J.H.S. Lee, I.O. Moen, *Prog. Energy Combust. Sci.* 6 (1978) 359–389.
[17] A.M. Khokhlov, E.S. Oran, *Combust. Flame* 119 (1999) 400–416.
[18] E.S. Oran, A.M. Khokhlov, *Philos. Trans. R. Soc. Lond. A* 357 (1999) 3539–3551.
[19] A.M. Khokhlov, E.S. Oran, G.O. Thomas, *Combust. Flame* 117 (1999) 323–339.
[20] V.N. Gamezo, A.M. Khokhlov, E.S. Oran, *Combust. Flame* 126 (2001) 1810–1826.

[21] A.M.J. Khokhlov, *J. Comput. Phys.* 143 (1998) 519–543.
[22] V.N. Gamezo, E.S. Oran, *AIAA J.* 44 (2006) 329–336.
[23] V.N. Gamezo, A.M. Khokhlov, E.S. Oran, Proceedings of the 17th ICDERS (1999) paper 237.
[24] V.N. Gamezo, A.A. Vasil'ev, A.M. Khokhlov, E.S. Oran, *Proc. Combust. Inst.* 28 (2000) 611–617.
[25] A.M. Khokhlov, AIAA Paper 2004-0792.
[26] A.I. Gavrikov, A.A. Efimenko, S.B. Dorofeev, *Combust. Flame* 120 (2000) 19–33.
[27] V.I. Manzhalei, *Fizika Goreniya i Vzryva* 13 (1977) 470–472.
[28] J.D. Ott, E.S. Oran, J.D. Anderson, *AIAA J.* 41 (2003) 1391–1396.

Comments

Sergey Frolov, *Semenov Institute of Chemical Physics*, *Russia.* In his early experiments with DDT in tubes with spirals, Shohelhin discovered that the DDT length and time are proportional to tube diameter. You have shown that these parameters are proportional to squared diameters. Could you comment on it?

Reply. Our result is different because when we vary the channel width, we also proportionally change the obstacle size and the distance between obstacles.

•

Dr. Michael Kuznetsov, *Research Center Karlsruhe*, *Germany*. (1) Choked flame velocity in tubes with high blockage ratio at about 0.9 can be equal to sonic velocity in reactants, not in products. In this case, detonation can propagate backwards and then decay with re-initiation. Did you study these cases?

(2) If the flame achieves some velocity for choking regime close to artificial conditions, the deflagration-to-detonation transition process does not depend on the distance. It has stochastic nature.

Reply. (1) We did not systematically study cases with high blockage ratios, and did not observe flames propagating with quasi-steady-state velocities that would correspond to the relatively low sound speed in reactants. When detonations appear in our simulations, they usually propagate in all directions where unburned material is present. Occasionally, the detonation is unable to spread forward past the obstacle, and propagates mostly backwards along the funnel of unburned material near the bottom wall. This backward propagation is limited by the distance between obstacles.

(2) Stochastic variations of the distance to DDT that we occasionally observed were relatively small, probably because computational parameters are easier to control than experimental ones. We plan to study this issue more systematically.

•

Andrew Higgins, *McGill University*, *Canada*. The "choked" regime refers to combustion products leaving the front at sonic velocity in the wave-fixed reference frame (i.e., a CJ deflagration). In a closed-ended tube or a heavy obstacle laden tube, the particle velocity of the products is nearly zero with respect to the tube wall, such that, upon coordinate transformation, the combustion front moves as the sonic velocity of the products in the lab-fixed frame. In order to determine if the flame is in the "choked" regime for the present simulations, it is necessary to compute the 1-D cross-section averaged Mach number of the flow in the wave-fixed frame.

Reply. It is obvious that the difference between the velocity of the combustion front and the velocity of burned material far behind does not depend on the frame of reference. For choking regimes considered here, this difference is close to the sound speed in combustion products. It is not obvious, however, that the thermal choking is the mechanism that limits the speed of the combustion front and the leading shock in channels with obstacles. In any case, there are several types of choking phenomena in gas dynamics that can be analyzed in relation with the "choking" regime of flame propagation. This issue deserves an extended discussion which is beyond the scope of this paper.